Step-decorated Ferromagnetic Fe Nanostripes on Pt(997)

Ruihua Cheng, K. Yu. Guslienko, F. Y. Fradin, J. E. Pearson, H. F. Ding, Dongqi Li, and S. D. Bader
Materials Science Division and Center for Nanoscale Materials, Argonne National Laboratory, Argonne, Illinois 60439, USA
(Received 1 February 2005; published 5 July 2005)

We investigate the step decoration growth and magnetic properties of Fe grown on a Pt(997) vicinal single crystal by means of reflection high energy electron diffraction (RHEED), scanning tunneling microscopy (STM), and the surface magneto-optical Kerr effect (SMOKE). Pt(997) has 2 nm wide, (111)-oriented terraces separated by ordered, monoatomic steps along the $[1\bar{1}0]$ direction. The Fe is grown at room temperature as wedges with thickness ranging from 0 to 4 monolayers (ML). RHEED and STM show that Fe stripes form at low coverage due to step decoration. SMOKE data taken along a wedge indicate that the Fe is ferromagnetic above 0.2 ML with its magnetic easy axis canted from surface normal direction. As temperature is increased near the Curie temperature, there is an irreversible spin reorientation to the perpendicular out-of-plane direction. The canting can be understood as arising from a competition between an in-plane, step-induced magnetic anisotropy and a perpendicular surface anisotropy associated with extended terraces due to the polarization of the proximal Pt. Above 1.7 ML the perpendicular easy axis reorients to in-plane, along the step direction, due to the dominance of the shape anisotropy. The magnetic anisotropy energy is extracted by fitting the temperature dependence of the coercivity data.

DOI: 10.1103/PhysRevB.72.014409 PACS number(s): 75.75.+a, 75.30.Gw, 75.70.Rf

INTRODUCTION

Magnetism in low-dimensional epitaxial systems is of great basic and applied interest.[1] While extensive progress has been made to understand magnetic films, our knowledge of one-dimensional (1D) ferromagnetism is limited. It is well known that an isolated 1D chain with isotropic finite-range exchange interactions cannot maintain long-range ferromagnetic order at finite temperature.[2,3] However, the presence of magnetic anisotropy, finite size, and/or nonequilibrium effects could break the symmetry and affect this conclusion.[2] Experimentally, it is possible to grow 1D nanostripes[4–8] and monoatomic chains[9] of transition metals on stepped surfaces by molecular beam epitaxy (MBE). Pioneering work by Elmers *et al.*[4] demonstrates that Fe/W(110) exhibits an onset of ferromagnetism at a stripe width of 0.8 nm (four atomic chains) with an in-plane magnetic easy axis perpendicular to the stripe direction. Li *et al.*[7,8] reported that Fe stripes grown on stepped Pd(110) are ferromagnetic above 0.3 monolayer (ML) coverage (corresponding to 0.6 nm wide stripes) and that the magnetic easy axis is along the surface normal. Above 0.7 ML the Fe easy axis starts to reorient in-plane along the step edge. The Curie temperature (T_C) vs. coverage exhibits the finite-size scaling of a 2D Ising system. Gambardella *et al.*[9] observed 1D ferromagnetism at $\sim 15 \pm 5$ K in monatomic Co chains grown on a Pt(997) surface due to the presence of magnetic anisotropy energy barriers. There has also been recent theoretical interest. The magnetic moment of monatomic Co on Pd(110) is calculated to be enhanced with respect to both the Co monolayer and Co bulk due to electronic localization.[10] Also, the magnetic anisotropy energy (MAE) of a 1D infinite chain is calculated to be an order of magnitude larger than that for 2D thin films.[11,12] Wu *et al.* calculated the MAE of monoatomic Co on different substrates and found that the MAE of Co is enhanced from 0.02 meV/atom on Cu(001) to 2.58 meV/atom on Pt(001) due to the strong spin-orbit coupling of Pt.[13]

In the present work we explore both the growth mode and magnetic properties of Fe grown on a Pt(997) surface in the coverage range of 0–4 ML. The vicinal Pt(997) surface has straight atomic step arrays with a narrow terrace width distribution attributed to repulsive interactions between adjacent steps.[14] Pt is known to be nearly ferromagnetic and can have an induced magnetic moment when in proximity to 3*d* ferromagnetic atoms. We use both scanning tunneling microscopy (STM) and reflection high-energy diffraction (RHEED) to monitor the Fe growth. Initially the growth proceeds via step decoration, and then islanding ensues above 2 ML. We find that the magnetic easy axis reorients from being in-plane (parallel to the step direction) to out-of-plane with decreasing Fe coverage. The Fe is ferromagnetic for coverage >0.2 ML above 35 K (the lowest temperature accessible in our experiments) and the magnetic easy axis is canted from the surface normal direction for submonolayer Fe coverage. As T is raised to approach T_C, the easy axis reorients irreversibly to the surface normal direction. Finally, the temperature dependence of the coercivity can be interpreted in terms of thermally activated, nonequilibrium spin dynamics of Fe nanostripes, and the anisotropy energy can be extracted by fitting the $H_C(T)$ data.

EXPERIMENTAL APPROACH

The experiments were carried out in an ultrahigh vacuum (UHV) MBE chamber with base pressure $<5\times10^{-11}$ Torr. The system is equipped with a STM, the surface magneto-optical Kerr effect (SMOKE), Auger electron spectroscopy, low-energy electron diffraction (LEED), and RHEED. The Pt(997) vicinal surface was created by cutting a Pt(111) crystal at an angle that is 6.5° offset to obtain atomic height steps along the $[1\bar{1}0]$ separated by terraces of ~ 2 nm average width, as schematically shown in Fig. 1(a). The Pt(997) was

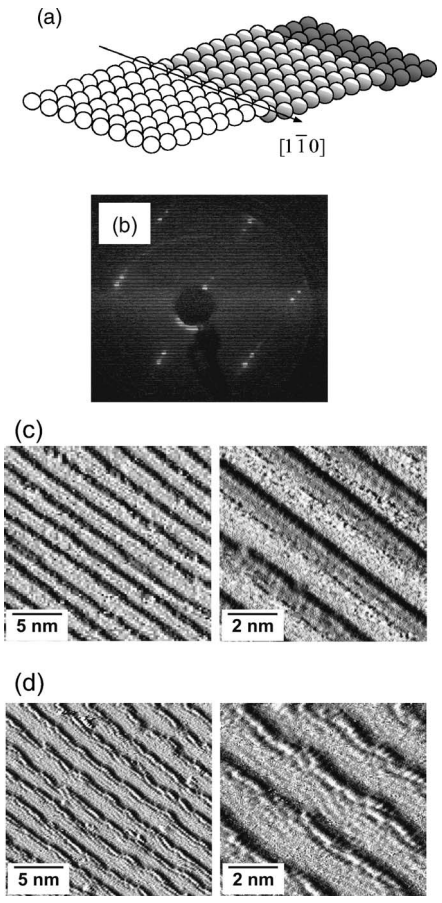

FIG. 1. (a) The schematic graph of the Pt(997) surface; (b) the LEED pattern of clean Pt(997) (taken at an electron energy of 79.8 eV); (c) the STM images of clean Pt(997) displayed in the derivative mode; and (d) the STM images of 0.15 ML Fe on Pt(997), displayed as in (c).

cleaned *in situ* with repeated cycles of Ar sputtering at 900 eV followed by annealing at 1000 K. The substrate was also occasionally annealed in oxygen at 5×10^{-8} Torr for a few minutes to eliminate surface carbon impurities. The resultant substrate is free of oxygen and carbon contamination within the Auger detection limit. Once the surface is atomically clean, Fe is deposited at room temperature with a low dose rate equivalent to 0.2 ML min^{-1}, as calibrated by both RHEED and STM. During the deposition the chamber pressure was $<2\times10^{-10}$ Torr. An Fe wedge was grown in the thickness range of 0–4 ML. The sample was then cooled to 35 K and SMOKE was used to study the magnetic properties along the wedge. The length of the wedge is 4 mm and the focused He-Ne laser beam size is 0.2 mm. Thus, the thickness gradient sampled for each SMOKE datum point corresponds to ±0.1 ML.

RESULTS AND DISCUSSION

Experimental data

The LEED pattern of the clean substrate is shown in Fig. 1(b). The image shows sharp, split spots. The split diffraction spots collapse into singlets as the electron beam energy is varied in a manner that is an indication of ordered arrays of atomic steps (with adjacent terraces exhibiting constructive and destructive interference as the beam energy varies). There is no other sign of reconstruction and the background is negligible. The distance between the split spots yields an average terrace width of $8\sim9$ atomic spacing. An *in situ* STM image of the clean Pt(997) surface is shown in Fig. 1(c). All STM images are displayed in the derivative mode (dz/dx) to highlight the step edges (where z is the height in a constant tunneling-current scan mode, and x is measured in-plane). The surface shows uniform steps with narrow deviations indicating a high-quality substrate. Step decoration growth of Fe on Pt(997) is observed at room temperature, as shown in the STM image for 0.15 ML of Fe/Pt(997) in Fig. 1(d). At this coverage, 1D Fe atomic chains form along the step edges without intermixing with the Pt substrate. At higher Fe coverage, the STM image shows similar features with wider chains. The growth was also studied by monitoring the RHEED intensity oscillations, as shown in Fig. 2(a) (with the recorded regions indicated in the inset). Figure 2(b) shows the RHEED patterns at different Fe coverages. The RHEED incident plane is parallel to the $[1\bar{1}0]$ step edge direction, so a typical RHEED pattern of the clean Pt(997) surface [inset of Fig. 2(a)] shows doublets. As the Fe is deposited, multiple features appear in the streaks, as shown in Fig. 2(b), due to the different scattering factors for Fe and Pt.[15] The sharp RHEED patterns indicate the initial smooth, layer-by-layer growth that results from step decoration. Above 2 ML the streaks start to blur and break into spots, indicating 3D growth. This is consistent with the decreased RHEED intensity shown in Fig. 2(a). The lattice relaxation (not shown here) of Fe grown on Pt(997) was studied by analyzing a series of RHEED patterns. According to the RHEED data, the first atomic layer of Fe grows pseudomorphically on the Pt(997) substrate. The Fe then gradually relaxes as it approaches a thickness of 4 ML. This is due to the large lattice mismatch of 10.6% between Fe and Pt.

Both longitudinal and polar SMOKE measurements were performed in order to characterize the magnetic properties, although only polar data are shown in this paper. For the longitudinal geometry the magnetic field was applied in-plane along the step edge $[1\bar{1}0]$, while for the polar geometry the magnetic field was applied normal to the surface, which is also perpendicular to the $[1\bar{1}0]$ step edge. The Kerr signal in remanence is proportional to the remanent magnetization M_r. Figure 3 illustrates magnetic hysteresis loops measured at 60 K at different Fe coverages. (The linear background slope of the loops is from the UHV window or paramagnetic impurities in the substrate.) The same 1 ML Fe loop in both figures serves as a reference. At Fe coverages >2 ML, only longitudinal hysteresis loops are observed, the polar signal being vanishingly small, as shown in Fig. 3(a). The magnetic easy axis is in-plane along the $[1\bar{1}0]$. We attribute this to the shape anisotropy and the induced magnetic anisotropy associated with the step edges,[16] although in-plane anisotropy perpendicular to the step edge has also been observed in other systems.[17,4,18] As the Fe coverage decreases, the polar M_r first increases, as illustrated in Fig. 3(a), exhibiting full

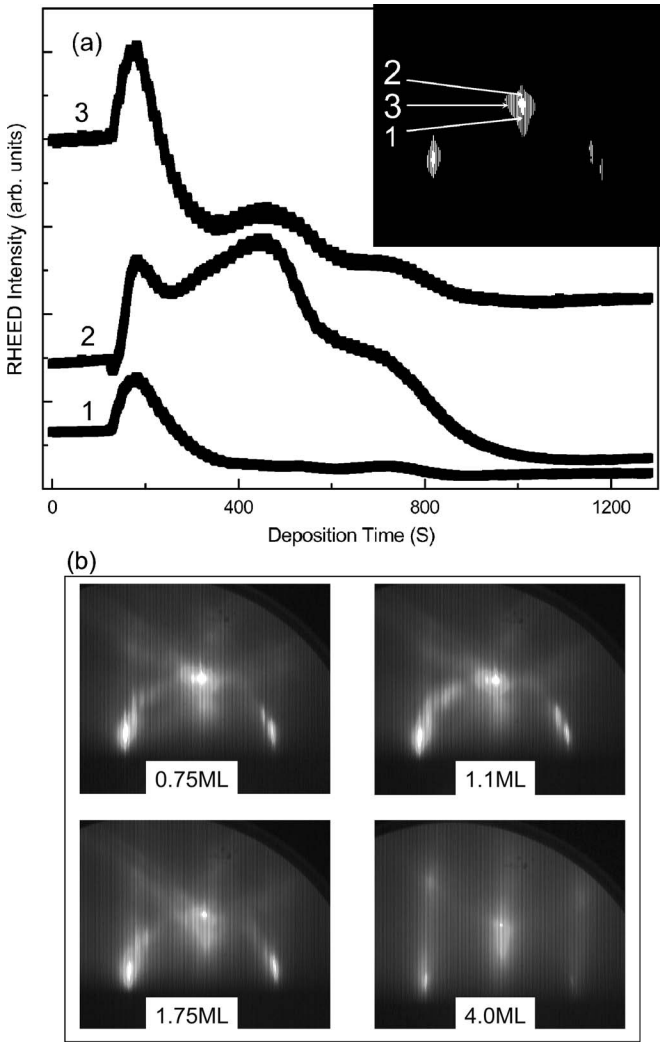

FIG. 2. (a) The RHEED intensities of Fe growing on Pt(997) at room temperature, taken at the locations indicated in the inset. The RHEED pattern shows split stripes because the incident plane is parallel to the $[1\bar{1}0]$ step direction. (b) The RHEED images of Fe on Pt(997) at the indicated Fe coverages.

remanence at ~1.7–1.8 ML, and then it decreases due to the decreased amount of Fe. The spin reorientation from in-plane to perpendicular starts to occur at 2 ML Fe and becomes out-of-plane at 1.7 ML, thus, Fe/Pt(997) appears to have a stronger surface anisotropy compared to Fe/Pd(110),[7] for which the spin reorientation occurs at 0.7 ML. The easy axis is canted away from the surface normal for submonolayer Fe coverages, based on the polar Kerr loops shown in Fig. 3(b). The loops are not square and do not exhibit full remanence even at the largest applied field. This agrees with the study of the angular dependence of the magnetization of Co atomic chains on Pt(997),[9] as well as theoretical calculations,[19] where it is reported that the easy axis is canted 20° from the perpendicular direction. The canting can be understood as arising from a competition between an in-plane, step-induced magnetic anisotropy and a perpendicular surface anisotropy associated with extended terraces due to the polarization of the proximal Pt.

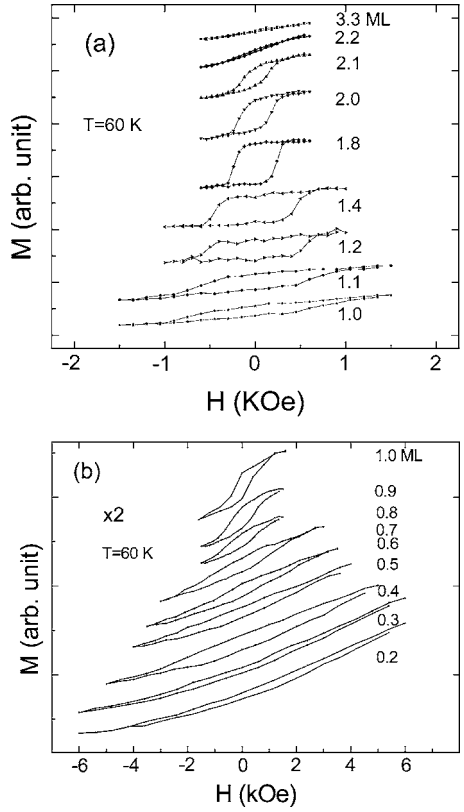

FIG. 3. The polar Kerr hysteresis loops at 60 K for Fe/Pt(997) at the indicated Fe coverages. [Note that the ordinate scale in (b) is 2× that in (a).]

The Fe/Pt(997) exhibits ferromagnetism down to 0.2 ML coverage presumably due to the step-induced magnetic anisotropy and proximal polarization of the Pt enabled by the step decoration. An important source of the large magnetic anisotropy of the Fe-Pt system is that the Pt contributes a strong spin-orbit interaction that couples to the Fe via $3d$-$5d$ hybridization. This behavior differs from that anticipated for island growth for which magnetic percolation occurs at ~0.6 ML coverage, as for Fe/W(110).[4] Our striped Fe system possesses finite coercivity and remanence on the time scale of our experiments, presumably due to the strong uniaxial anisotropy and the correspondingly high-energy barriers that prevent the system from reaching equilibrium. Although the out-of-plane anisotropy of Fe/Pt(997) might result in antiferromagnetic ordering of adjacent stripes due to dipolar interactions,[20,21] no sign of this was observed. We attribute this to the strong ferromagnetic polarization of the Pt substrate and the nonequilibrium effect.

Figure 4 shows the Fe coverage dependence of M_r and H_C measured as a function of temperature. Two insights can be drawn from the data, as we will now describe. First, consider that at the spin reorientation transition (SRT) temperature, T_{SR}, the perpendicular surface anisotropy field compensates the demagnetizing field,[22] $2K_s(T)/M_s d_{SR}=4\pi D_{eff} M_s$, where d_{SR} is the Fe coverage at the transition and D_{eff} is the effective demagnetization factor. Because d_{SR} is independent of T in the 60–300 K range, as illustrated in Fig. 4(a), this implies that the perpendicular surface anisotropy K_s has a T depen-

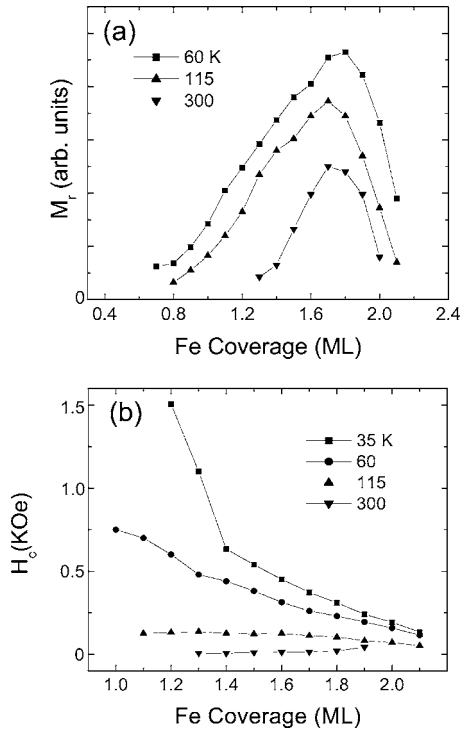

FIG. 4. The Fe coverage-dependent (a) remanent magnetization M_r and (b) coercivity H_C of Fe/Pt(997) measured via the polar Kerr effect at the indicated temperatures.

dence that varies as $K_s(T) \propto M_s^2(T)$. A similar T dependence of the anisotropy constant was recently calculated for bulk ordered $L1_0$ phase *fct* FePt due to the anisotropic Fe-Fe exchange coupling via the polarized Pt atoms.[23] Second, consider that H_C is related to domain nucleation and domain wall pinning, as well as to the magnetic anisotropy. The domains here are strongly correlated blocks of spins directed up or down with respect to the anisotropy axis. The blocks are coupled via the exchange interaction and separated by domain walls. The magnetization reversal occurs via field- and thermally activated wall movement along the Fe stripes. Such spin-block dynamics, known as Glauber dynamics, can be described within a nonequilibrium 1D Ising model. As shown in Fig. 4(b), at low T within the coverage range of $1 < \theta < 2.1$ ML, H_C increases with decreasing Fe coverage, while at higher T, it shows less coverage dependence. This can be understood as arising from two mechanisms. One is that as T approaches T_C, H_C decreases due to thermally activated depinning. The other mechanism is that the decrease of H_C with increasing Fe coverage results from a nonuniformity of the stripe width.[24] The domain walls are pinned at constrictions along the stripes at low coverage. Increasing the Fe coverage would lead to an unblocking of the constrictions, depinning the domain walls and reducing H_C. This picture has been confirmed by spin-polarized tunneling spectroscopy measurements by Pietzsch *et al.*,[25,26] where two kinds of domain walls with average widths of 2 and 6 nm were observed in Fe/W(110). However, strain could dominate the energetics in other systems, such as Fe on vicinal Ag(001).[27]

We also performed T-dependent M_r and H_C measurements, as shown in Fig. 5. For an Fe coverage of 1.1 ML, M_r

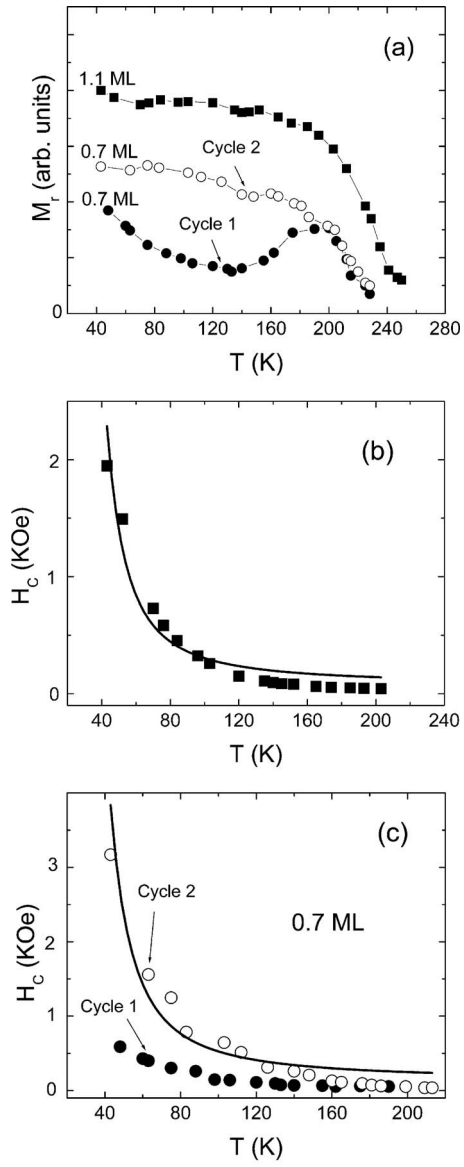

FIG. 5. The remanence M_r (a) and coercivity H_C (b, c) of Fe/Pt(997) films vs. T at the indicated Fe coverages. The solid lines in (b) and (c) are the exponential fits to the experimental data according to Eq. (2).

vs. T yields $T_C \sim 250$ K, as shown in Fig. 5(a). However, for 0.7 ML Fe, M_r vs. T shows a T-dependent SRT close to T_C. The SRT is irreversible, as illustrated by the two measurement cycles in Fig. 5(a). As mentioned earlier, the magnetization is canted away from the surface normal for submonolayer Fe coverages. With increasing T [cycle 1 in Fig. 5(a)], first M_r decreases, and then it starts to increase at 150 K and reaches a peak at 190 K. This indicates that the easy axis is canted below 150 K; then it reorients perpendicular to the surface with full remanence on further warming. Repeating the measurement, we find that the SRT is irreversible, as shown in cycle 2 in Fig. 5(a). H_C is dramatically enhanced in cycle 2 compared with cycle 1 due to this transition. The irreversibility of the SRT might be due to the canted easy axis being metastable compared to the surface normal axis. When the sample is heated it overcomes the energy barrier

and the easy axis is stabilized in the perpendicular (surface normal) direction. Another possible explanation would be that the SRT could be induced by surface adsorbates. Cycle 2 followed cycle 1, taking several hours of measurement time, so the surface could adsorb residual gas molecules. Experimental[24,28] and theoretical[29] studies confirm that adsorbates can induce a SRT. We will explore this question further in the future for our experimental system and conditions.

The H_C vs. T data for both 1.1 and 0.7 ML provide exponential decay information, shown in Fig. 5(b). From our prior discussion, we know that between 60 and 300 K the surface anisotropy K_s depends on T as $K_s(T) \propto M_s^2(T)$, thus we conclude that the main contribution of H_C vs. T is not due to the T dependence of the anisotropy.

Model of dynamical coercivity

To evaluate the T dependence of H_C we apply the equation of magnetization motion in the form provided by Glauber.[30] We assume that a spin-block that is N atoms long can be represented as a single "super" spin due to strong exchange coupling within the block. The equation of motion within the mean-field approximation for the super-spin $N\mu$ is

$$\tau \frac{dm}{dt} = -m + \tanh[\beta(h + Jm)], \tag{1}$$

where μ is the magnetic moment of the stripe segment, τ is the spin-block relaxation time, $m = \langle M_z \rangle / N\mu$ is the T-averaged reduced magnetic moment along the $+z$ direction, $h = \mu H_z$, $J = zJ_0$, z is the number of neighbors for a given Fe atom ($z=2$ for a chain of Fe atoms along the step edge), J_0 is the exchange integral between neighbors, and $\beta = 1/k_B T$.

We assume that at the external field of finite sweep-rate dH_z/dt can be modeled by an oscillating field $h(t) = h_0 \cos(\omega t)$ with frequency ω. Equation (1) can then be solved and it can be shown that in the low-frequency limit ($\omega\tau \ll 1$) the dynamic coercive field is $H_c \sim \omega\tau$. This approximation is well justified because the frequency of the experimental hysteresis loop measurements is about 10^{-3} Hz and the relaxation time of the spin blocks τ does not exceed 10–100 ns within the experimental temperature range ($T > 40$ K). The relaxation time of flipping between up and down directions in the double-well potential of the uniaxial anisotropy can be represented as $\tau = \tau_0 \exp(\beta N K_1)$, where K_1 is the anisotropy energy per chain segment (per atom for a one-atom wide chain). The average length of spin block N at given T can be represented, in general, as a sum of two different contributions $N(T) = \bar{N} + N_d(T)$, where $\bar{N}$ is a static contribution and $N_d(T)$ is the contribution of the dynamical fluctuations. $N_d(T)$ can be estimated from the correlation length of the 1D Ising model[3] $\xi(T) = a\{\ln[\coth(\beta J_0)]\}^{-1}$, where a is the lattice period along the stripes. Thus, the temperature-dependent coercivity can be written in an exponential form as

$$H_C(T) = H_0 \omega \tau_0 \exp\left(\frac{T_K}{T} N(T)\right), \tag{2}$$

TABLE I. Magnetic anisotropy energy determined by fitting the Fe/Pt(997)$H_c(T)$ data

Fe coverage (ML)	$T_0 = NK_1/k_B$ (K)	$\Delta E = NK_1$ (10^{-14} erg)	Anisotropy energy per Fe atom, K_1/N_x (meV/Fe atom)	N_x
0.7 (Cycle 2)	158	2.18	0.151	6
1.1	163	2.25	0.094	10

$$N(T) = \bar{N} + N_d(T), \quad N_d(T) = \ln^{-1}\left[\coth\left(\frac{T_e}{T}\right)\right],$$

$$T_K = K_1/k_B, \quad T_e = J_0/k_B,$$

where H_0 and τ_0 vary slowly with T. We can use Eq. (2) to fit the experimental $H_c(T)$ data. This enables us to obtain approximate values for the energy barrier $\Delta E(T) = N(T)K_1$, the anisotropy K_1, and the anisotropy energy per Fe atom in the chain. Equation (2) corresponds to a very sharp temperature dependence of $H_C(T)$, which was observed in Fe/W(110).[24] The fitting depends on the Fe-Fe exchange integral J_0 which is not a well-defined parameter for Fe (or Co) nanochains or nanostripes. Gambardela *et al.*[9] estimated that $J_0 = 7.5$ meV for Co chains on Pt, whereas Brown *et al.*[31] estimated the exchange integral as $J_{\text{Fe-Fe}} = 2$ meV for Fe nanostripes on Cu(111). Shen *et al.*[15] determined that $T_e < 100$ K ($J_0 < 8.6$ meV) by fitting hysteresis loops for Fe/Cu(111). All these values are essentially smaller than the bulk exchange integrals for 3d ferromagnets (of order of 100 meV). We use the definition of $J_{\text{Fe-Fe}} = J_0/N_x$, where N_x is the number of Fe atoms along a Pt terrace (Fe-nanostripe width). Note that $N_x = 6$ corresponds to 0.7 ML, and $N_x = 10$ for 1.1 ML coverage. Fitting the experimental $H_C(T)$ data we varied the exchange integral within the range 1–20 meV and concluded that the $\bar{N}$ term of the spin-block length dominates and the $N_d(T)$ term related to exchange can be neglected in the first approximation for the temperature range 40–230 K. The fitting results are shown as solid lines in Figs. 5(b) and 5(c) and are collected in Table I. The above equations apply for the magnetic easy axis, so we only use the cycle 2 data to do the analysis for the 0.7 ML sample. The $\bar{N} = 15$ was estimated in Ref. 9 for Co chains on Pt, and we used this value to recalculate the energy barriers and anisotropy parameters per Fe atom. As expected, the anisotropy energy for 0.7 ML Fe is higher than that for the 1.1 ML Fe data. For 0.7 ML Fe coverage corresponding to 1.4 nm wide stripes ($\sim$6 Fe atoms wide), our value of $K_1/N_x \sim 0.151$ meV/atom is $\sim$50 times the bulk Fe anisotropy energy (of ~ 3.5 μeV/atom[32]) and is comparable to that reported for the Fe on stepped W(001) system.[33] This effect is related to the considerable increase of the orbital moment of confined Fe in comparison that of the bulk. The magnetic anisotropy energy per Fe atom decreases with increasing stripe width (as shown in the last column of Table I). Our estimation of the anisotropy energy per Fe atom in Fe/Pt(997) nanostripes as 0.1–0.2 meV could be com-

pared with future *ab initio* calculations of the anisotropy parameter K_1.

The above analysis, yielding an exponential dependence of $H_C(T)$, reveals that the magnetization reversal mechanism is governed by thermally activated, nonequilibrium magnetization dynamics of the Fe stripe segments in a magnetic field. The spin-block length cannot be considered as a purely dynamical variable; pinning of the Fe domains (spin segments) on the nanoscale due to the film morphology plays an essential role. The nanostripes have structural constrictions as shown in Figs. 1(c) and 1(d). Pietzsch *et al.*[25] observed the onset of narrow domain walls (with width ~2 nm) localized in constricted parts of Fe nanostripes on W(110). The constrictions in the nanostripes serve as pinning centers for domain walls, govern the length of the Fe-domain stripe segments, and explain the small contribution of the intersegment exchange interaction in the coercivity model described above by Eq. (2). The stripe segments respond to the external field almost independently.

CONCLUSIONS

We investigated the growth and magnetic properties of Fe grown on a Pt(997) vicinal single crystal surface at room temperature in a wedge geometry with thickness ranging from 0 to 4 ML. Both monolayer-range Fe films and submonolayer-range Fe step-decorated stripes were studied. There is a temperature-independent spin reorientation from in-plane along the step edges to out-of-plane as Fe coverage decreases below 2 ML. The magnetic easy axis of the stripes is canted away from the perpendicular (surface-normal) direction at low temperature. However, it irreversibly reorients and is stabilized out-of-plane close to T_C. The coercivity of both the monolayer-range films and submonolayer, step-decorated stripes fit an exponential decay with temperature that can be understood as being due to thermally activated, nonequilibrium spin dynamics of the Fe nanostripes formed at the Pt-substrate steps. Finally, the magnetic anisotropy energy per Fe atom for different Fe coverages is extracted by fitting the experimental temperature-dependent coercivity data.

ACKNOWLEDGMENTS

This work was supported by the US DOE BES-Materials Sciences under Contract No. W-31-109-ENG-38. SDB and HD acknowledge the University of Chicago-Argonne Consortium for Nanoscience Research.

[1] F. J. Himpsel, J. E. Ortega, G. J. Mankey, and R. F. Willis, Adv. Phys. **47**, 511 (1998).
[2] N. D. Mermin and H. Wagner, Phys. Rev. Lett. **17**, 1133 (1966).
[3] J. M. Yeomans, *Statistical Mechanics of Phase Transitions* (Clarendon Press, Oxford, 1992), Chap. 5.
[4] H. J. Elmers, J. Hauschild, H. Hoche, and U. Gradmann, H. Bethge, D. Heuer, and U. Köhler, Phys. Rev. Lett. **73**, 898 (1994).
[5] J. Shen, R. Skomski, M. Klaua, H. Jenniches, S. Sundar Manoharan, and J. Kirschner, Phys. Rev. B **56**, 2340 (1997); J. Shen, R. Skomski, M. Klaua, H. Jenniches, S. Sunder Mankharan, and J. Kirschner, J. Appl. Phys. **81**, 3901 (1997).
[6] G. Benedek, B. Hulpke, and W. Steinhogl, Phys. Rev. Lett. **87**, 027201 (2001).
[7] D. Li, B. R. Cuenya, J. Pearson, S. D. Bader, and W. Kuene, Phys. Rev. B **64**, 144410 (2001).
[8] B. Roldan Cuenya, J. Pearson, Chengtao Yu, Dongqi Li, and S. D. Bader, J. Vac. Sci. Technol. A **19**, 1182 (2001).
[9] P. Gambardella, A. Dallmeyer, K. Maiti, M. C. Malagoli, W. Eberhardt, K. Kern, and C. Carbone, Nature (London) **416**, 301 (2002); P. Gambardella, A. Dallmeyer, K. Maiti, M. C. Malagoli, S. Rusponi, P. Ohresser, W. Eberhardt, C. Carbone, and K. Kern, Phys. Rev. Lett. **93**, 077203 (2004).
[10] R. Robles, J. Izquierdo, and A. Vega, Phys. Rev. B **61**, 6848 (2000).
[11] J. Dorantes-Dávila and G. M. Pastor, Phys. Rev. Lett. **81**, 208 (1998); J. Dorantes-Dávila, H. Dreyssé, and G. M. Pastor, *ibid.* **91**, 197206 (2003).
[12] R. Félix-Medina, J. Dorantes-Dávila, and G. M. Pastor, New J. Phys. **4**, 1001 (2002).
[13] J. Hong and R. Q. Wu, Phys. Rev. B **67**, 020406(R) (2003).
[14] S. Papadia, M. C. Desjonqueres, and D. Spanjaard, Phys. Rev. B **53**, 4083 (1996).
[15] P. K. Larsen and P. J. Dobson, in *Reflection High-Energy Electron Diffraction and Reflection Electron Imaging of Surfaces*, NATO Advanced Studies Institute, Series B: Physics (Plenum, New York, 1987), Vol. 188.
[16] A. Berger, U. Linke, and H. P. Oepen, Phys. Rev. Lett. **68**, 839 (1992).
[17] H. J. Choi, R. K. Kawakami, E. J. Escorcia-Aparicio, Z. Q. Qiu, J. Pearson, J. S. Jiang, Dongqi Li, and S. D. Bader, Phys. Rev. Lett. **82**, 1947 (1999).
[18] Y. Z. Wu, C. Won, H. W. Zhao, and Z. Q. Qiu, Phys. Rev. B **67**, 094409 (2003).
[19] Alexander B. Shick, František Máca, and Peter M. Oppeneer, Phys. Rev. B **69**, 212410 (2004).
[20] J. Hauschild, H. J. Elmers, and U. Gradmann, Phys. Rev. B **57**, R677 (1998).
[21] Ya. B. Losovyj, I. N. Yakovkin, H. K. Jeong, David Wisbey, and P. A. Dowben, J. Phys.: Condens. Matter **16**, 4711 (2004).
[22] B. Heinrich, J. F. Cochran, A. S. Arrott, S. T. Purcell, K. B. Urquhart, J. R. Dutcher, and W. F. Egelhoff, Appl. Phys. A: Solids Surf. **49**, 473 (1989).
[23] O. N. Mryasov, U. Nowak, K. Yu. Guslienko, and R. Chantrell, Europhys. Lett. **69**, 805 (2005).
[24] H. J. Elmers, J. Hauschild, and U. Gradmann, Phys. Rev. B **59**, 3688 (1999).
[25] O. Pietzsch, A. Kubetzka, M. Bode, and R. Wiesendanger, Phys. Rev. Lett. **84**, 5212 (2000).
[26] M. Bode, A. Kubetzka, O. Pietzsch, and R. Wiesendanger, Surf. Sci. **514**, 135 (2002).
[27] Y. Z. Wu, C. Won, and Z. Q. Qiu, Phys. Rev. B **65**, 184419 (2002).

[28] D. Matsumura, T. Yokoyama, K. Amemiya, S. Kitagawa, and T. Ohta, Phys. Rev. B **66**, 024402 (2002).
[29] B. Újfalussy, L. Szunyogh, P. Bruno, and P. Weinberger, Phys. Rev. Lett. **77**, 1805 (1996).
[30] K. H. Fischer and J. A. Hertz, *Spin Glasses* (Cambridge University Press, New York, 1991).
[31] G. Brown, H. K. Lee, T. C. Schulthess, B. Ujfalussy, G. M. Stocks, W. H. Butler, D. P. Landau, J. P. Pierce, J. Shen, and J. Kirschner, J. Appl. Phys. **91**, 7056 (2002).
[32] D. Sander, J. Phys.: Condens. Matter **16**, R603 (2004).
[33] A. Kubetzka, O. Pietzsch, M. Bode, and R. Wiesendanger, Phys. Rev. B **63**, 140407 (2002).